Chemical Science

ROYAL SOCIETY OF CHEMISTRY

EDGE ARTICLE

View Article Online
View Journal

Check for updates

Cite this: DOI: 10.1039/d5sc04153h

All publication charges for this article have been paid for by the Royal Society of Chemistry

Rapid nitrite reduction enabled by secondary sphere hydrogen bonds within non-heme iron complexes

Andrew R. LaDuca, [a] Jared E. Gonder, [a] Writhabrata Sarkar, [a] John D. Gilbertson *[b] and Nathaniel K. Szymczak *[a]

Received 6th June 2025
Accepted 28th August 2025

DOI: 10.1039/d5sc04153h

rsc.li/chemical-science

A non-heme iron(II) complex bearing a ligand with secondary sphere hydrogen bond (H-bond) donors, (tris(6-phenylaminopyridylmethyl)amine, TPA^{NHPh}, rapidly reduces nitrite (NO_2^-) to nitric oxide (NO) in the absence of exogenous additives, affording a $Fe(III)_2(\mu\text{-}O)_2$ diamond core. An electronically analogous complex containing a ligand without H-bonds (tris(6-methylpyridylmethylamine), TPA^{Me}, also reduces NO_2^- to NO and forms an $Fe(III)_2(\mu\text{-}O)_2$ core, but is four orders of magnitude slower, highlighting the impact of H-bonds to promote NO_2^- reduction. We compare the structural and spectroscopic differences of the two $Fe(III)_2(\mu\text{-}O)_2$ complexes and show that H-bonding interactions weaken the Fe–O bonds, perturb the electronic structure of the Fe_2O_2 cores, and thereby engender distinct reductive stability profiles.

Introduction

Nitrite (NO_2^-) is a source for physiological production of nitric oxide (NO), which is an important bioregulatory signalling molecule.[1] NO has multiple functions as a vasodilator, neurotransmitter, and has important roles in mammalian immune responses.[1,2] In these biological contexts, an array of Fe- and Cu-based metalloenzymes (*e.g.* cytochrome cd1- or cytochrome c nitrite reductases, *cd1-NiR*/*cc-NiR*, and *Cu-NiR*) catalyze the reduction of NO_2^- to NO or to NH_3 (ccNiR).[3] Mutagenesis and computational studies implicate a critical role of specific hydrogen-bonding (H-bonding) amino acids close to the active sites of these enzymes (*i.e.*, in the secondary sphere) for enzymatic function.[4] Removal of these H-bonding residues in *cd1-* or *cc-NiR* inhibits catalytic activity, affording up to a 99% decrease in catalytic rates, highlighting their roles to both enable and accelerate enzymatic NO_2^- reduction.[5] Although the dependence on H-bonds for overall function is established, the molecular-level details of these interactions are challenging to clarify because removal induces larger structural changes, obfuscating their role(s) on individual reaction steps.[4a]

Inorganic model complexes can provide insight into the effects of secondary sphere H-bonds,[6] and by extension, the mechanisms of enzymatic NO_2^- reduction. Complexes that do not contain H-bond donors often require the addition of an exogenous Brønsted acid and/or (electro)chemical reducing equivalents to promote NO release.[7] In contrast, systems containing secondary sphere H-bond donors can induce spontaneous NO_2^- reduction without exogenous acids.[8] Seminal work by the Fout group reported facile NO_2^- reduction mediated by Fe in a tripodal azafulvine-imine ligand scaffold, producing NO and a monomeric Fe(III)–O(H), a result that was attributed to the

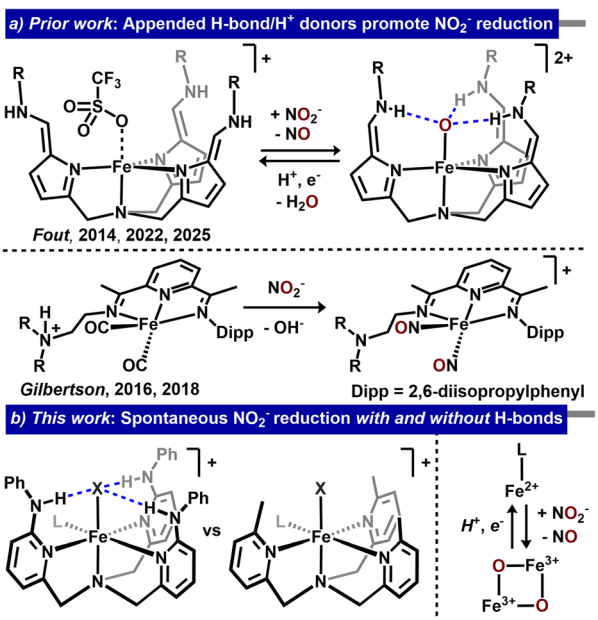

Fig. 1 (a) Previously reported Fe-based systems with secondary sphere H^+/H-bond donors that spontaneously reduce NO_2^-,[8b–d,9,10] (b) this work.

[a]Department of Chemistry, University of Michigan, Ann Arbor, MI, USA. E-mail: nszym@umich.edu

[b]Department of Chemistry, Western Washington University, Bellingham, WA, USA. E-mail: gilberj4@wwu.edu

pendent-imino groups acting as H-bond donors (Fig. 1a).[8b–d,9] Related reports from the Gilbertson group highlighted Fe-pyridinediimine complexes with tethered amines that reduced NO_2^- to afford an $\{Fe(NO)_2\}$[9,10] and the Hung group reported an N-confused porphyrin that similarly reduced NO_2^- to form an $\{Fe(NO)\}^{6/7}$.[11]

While these prior studies demonstrated synthetic examples of H-bond promoted NO_2^- reduction, direct comparisons between ligands that either contain or omit H-bonds are notably absent. Modification of the secondary sphere of a complex can impact its primary coordination sphere *via* perturbations to ligand field environments, redox potentials, or spin states.[5a,12] These competing effects present challenges when assessing the role(s) of H-bonds during NO_2^- reduction. Our group has attempted to decouple these parameters by comparing reaction outcomes with electronically similar ligands that differ in their secondary sphere,[13] and we previously showed that a scaffold containing aniline groups as H-bond donors, (tris(6-phenylaminopyridy-lmethyl)amine, TPA^{NHPh}), promoted capture/activation of O_2 (with Fe, Cu, and Zn)[13b,f,g] in addition to tandem ClO_4^- reduction/C–H oxygenation (with Fe).[13a,c] We also reported a Cu(I) complex with a related ligand containing appended OH groups, tris(6-hydroxypyridylmethyl)amine TPA^{OH}Cu(I), which reduced NO_2^- to NO, an example of ligand-promoted H^+/e^- transfer.[14] In this report, we expand these efforts to Fe-mediated NO_2^- reduction.

Results and discussion

Introduction of excess (*ca.* 10 equiv.) $[Bu_4N][NO_2]$ to an MeCN solution of TPA^{NHPh}Fe(II) bis(bis-trifluoromethylsulfonylazanide), ($TPA^{NHPh}Fe(NTf_2)_2$, **I-NTf$_2$**, Fig. 2a), under ambient conditions afforded a two-step reaction sequence: a rapid color change from colorless to yellow (seconds), followed by a gradual transition to reddish-brown (hours). Removal of MeCN *in vacuo* followed by precipitation from CH_2Cl_2/Et_2O provided a single product, as assessed by ^{1}H-NMR spectroscopy. A solution-phase IR spectrum of the product contained no Fe–NO stretches between 1600–1850 cm^{-1}, but did exhibit broadened and bathochromically shifted N–H stretches (ν_{NH} = 3232 and 3188 cm^{-1}) relative to **I-NTf$_2$** (ν_{NH} = 3361 and 3278 cm^{-1}), consistent with strengthened H-bond interactions.[15] To examine whether NO was released during this reaction, we allowed **I-NTf$_2$** to react with excess $[Bu_4N][NO_2]$ in the presence of CoTPP (TPP = tetraphenyl porphyrin), which provided quantitative yield of CoTPP(NO) after 5 h.[16] These data are consistent with spontaneous NO_2^- reduction to NO by **I-NTf$_2$**, potentially with concomitant formation of an Fe–O unit, as we did not observe Fe–NO bond formation.

To determine the molecular composition of the product, we performed a single-crystal X-ray diffraction (XRD) experiment on crystals grown from CH_2Cl_2/Et_2O. Rather than a monomeric Fe–O, the refined structure revealed a $[Fe(III)_2(\mu\text{-}O)_2]^{2+}$ diamond core (**II**, Fig. 2c) enveloped by moderate strength H-bonding interactions (average O_1–N_3 distance of 2.9 ± 0.2 Å).[17] This Fe_2O_2 structural motif is reminiscent of higher valent intermediates within non-heme di-iron enzymes (*e.g.* soluble

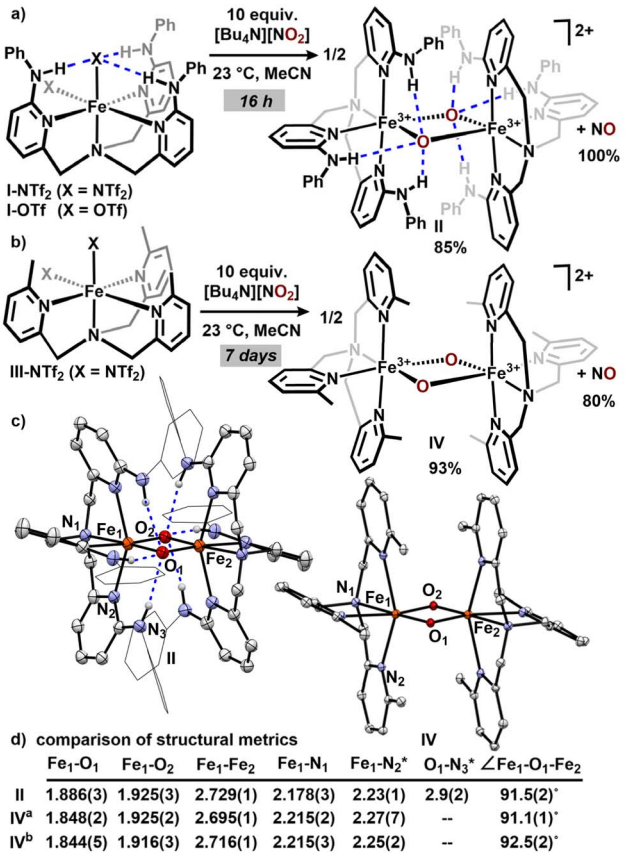

	Fe_1-O_1	Fe_1-O_2	Fe_1-Fe_2	Fe_1-N_1	Fe_1-N_2*	O_1-N_3*	∠Fe_1-O_1-Fe_2
II	1.886(3)	1.925(3)	2.729(1)	2.178(3)	2.23(1)	2.9(2)	91.5(2)°
IV[a]	1.848(2)	1.925(2)	2.695(1)	2.215(2)	2.27(7)	--	91.1(1)°
IV[b]	1.844(5)	1.916(3)	2.716(1)	2.215(3)	2.25(2)	--	92.5(2)°

Fig. 2 (a) Reaction of $TPA^{NHPh}Fe(x)_2$ (X = OTf^- or NTf_2^-; **I-OTf** or **I-NTf$_2$**) with NO_2^- to form NO(g) and $TPA^{NHPh}{}_2Fe(III)_2(\mu\text{-}O)_2^{2+}$ (**II**). (b) Reaction of $TPA^{Me}Fe(NTf_2)_2$ (**III-NTf$_1$**) with NO_2^- to form $TPA^{Me}{}_2Fe(III)_2(\mu\text{-}O)_2^{2+}$(**IV**) and $NO_{(g)}$, (c) molecular structures of **II** and **IV** (NO_2^--derived); 50% probability ellipsoids, short H-bond contacts highlighted in blue, phenyl groups are wireframed, H-atoms not involved in H-bonds, and outer sphere anions omitted for clarity (d). Bond metrics of **II**, **IV**[a] and **IV**[b] (a: this work, b: ref. 19*g*, *denotes an average of 3 bond distances).

methane monooxygenase (*sMMO*-Q) in the $Fe(IV)_2$ state and ribonucleotide reductase (*RNR*-X) in the Fe(III)Fe(IV) state)[18] but is comparatively rare in synthetic systems.[19] Que and coworkers reported the first isolated $Fe(III)_2(\mu\text{-}O)_2$ core, supported by two tris(6-methylpyridylmethyl)amine) ligands, ($TPA^{Me}{}_2Fe(III)_2(\mu\text{-}O)_2^{2+}$ **IV**), which was prepared *via* more standard oxygenation reagents (tBuOOH and NEt_3).[19g] Another related example, reported by Masuda, is a TPA^{NH_2} analogue that formed an H-bonded $Fe(III)_2(\mu\text{-}O)_2$ species from O_2.[19c] We found that **IV** could also be prepared directly from $[Bu_4N][NO_2]$, albeit over a longer time frame (1 week, Fig. 2b). Importantly, TPA^{Me} provides an analogous primary sphere environment as TPA^{NHPh}, but does not contain pendent H-bond donors.[13b] Thus, we propose that differences in the chemical properties of **II** and **IV** can be attributed to the effects of secondary sphere H-bonds.

The structural metrics in **II** are similar to those in **IV**, with a few notable exceptions (Fig. 2d).[20] The Fe_2O_2 diamond core in **II** displays two distinct Fe–O bonds (Fe_1–O_1: 1.886(3) Å, and Fe_1–

O_2: 1.925(3) Å), an Fe_1–Fe_2 separation of 2.729(1) Å, and an Fe_1–O_1–Fe_2 angle of 91.5(2)°. In comparison, **IV** has a 0.038(4) Å shorter Fe_1–O_1 bond (1.848(2) Å) and a 0.034(2) Å shorter Fe–Fe distance (2.695(1) Å), but the other Fe_2O_2 core metrical parameters are similar (Fe_1–O_2: 1.925(2) Å, and ∠Fe_1–O_1–Fe_2: 91.1(1)°). The elongated Fe_1–O_1 bond likely exhibits a weaker *trans*-influence, which is manifest by the contracted Fe_1–N_1 distance of **II** (2.178(3) Å) compared to **IV** (2.215(2) Å). We attribute these structural differences to the trifurcated H-bonds surrounding each μ-O^{2-} ligand in **II**, which are proposed to reduce the basicity of oxo ligands, thereby weakening the Fe–O bonds.[19c,21,22]

To clarify the electronic differences that are imparted by H-bonding interactions, we examined the electronic absorption spectra of **II** and **IV**. Their respective spectra are distinct: **II** exhibits a prominent shoulder band at 433 nm (ε = 2.6 mM^{-1} cm^{-1}) while **IV** displays a similarly intense shoulder band at 375 nm (ε = 2.0 mM^{-1} cm^{-1}), both assigned to LMCT transitions.[19b] These spectral shifts suggest that H-bonding interactions alter the electronic structure of the $Fe_2(\mu\text{-}O)_2$ cores, which we interrogated further by Mössbauer spectroscopy. The zero-field Mössbauer spectrum (Fig. 3, top) of **II** as a solid (at 298 K) displays a symmetric doublet with an isomer shift (δ) of 0.33 mm s^{-1} and quadrupole splitting (ΔE_q) of 1.422 mm s^{-1}, consistent with two identical high spin Fe(III) centers.[19a,23] These data are distinct from the reported Mössbauer parameters of **IV:** (symmetric, δ = 0.50 mm s^{-1}; ΔE_q = 1.93 mm s^{-1}). We attribute the differences in δ (lower δ for **II**) to more oxidized/Lewis acidic Fe(III) centers,[22] and the differences in ΔE_q values to H-bond induced charge redistribution and/or orbital rehybridization of the μ-O ligands.[24] These effects may also be partially responsible for the decrease in antiferromagnetic coupling in **II** (J = −28 cm^{-1}) relative to **IV** (J = −54 cm^{-1}).[19g,25]

The differences in electronic structures of the $Fe(III)_2(\mu\text{-}O)_2$ cores within **II** and **IV** allude to distinct redox behaviors, which we investigated by cyclic voltammetry (CV, Fig. 3, bottom). The CV of **II** exhibited three principal features: a reversible 1e^- reduction at −0.78 V (*vs.* $Fc^{0/+}$, assigned as a $Fe(III)_2$/$Fe(III)Fe(II)$ couple), and two irreversible events at −1.2 V and +0.92 V, see SI. The well-behaved reduction event of **II** is in stark contrast to **IV**, where the CV was not well-defined, and instead, displayed broad features with an E_{onset} = −0.80 V (Fig. 3, see SI).[28,29]

To probe differences in reductive stability, we evaluated chemical reductions of **II** and **IV**. The reaction of **II** with 1 equiv. Na^0 (as 5% Na/NaCl) in frozen THF afforded a mixture of products (as assessed by ^{1}H-NMR spectroscopy) but did not induce demetalation. An analogous reduction of **IV** underwent immediate demetalation, generating free ligand as the sole TPA^{Me} containing product. In contrast, introduction of milder reagents capable of delivering H^+/e^- equivalents (*i.e.* H-atom donors) provided tractable reactivity with both **II** and **IV**. Addition of 1.5 equiv. 1,2-diphenylhydrazine (DPH, $N\text{–}H_{BDFE}$ = 68 kcal mol^{-1})[30] to **II** (23 °C, MeCN) provided quantitative formation of $TPA^{NHPh}Fe(II)(OH)^+$ (**I-OH**, Fig. 4) and azobenzene after 24 h, a net $2H^+/2e^-$ reduction of **II**.[31] In comparison, addition of 1.5 equiv. DPH to **IV** immediately (*ca.* 15 min, 23 °C) produced a new species (assigned as $TPA^{Me}Fe(II)(H_2O)_x(\text{-MeCN})_y^{2+}$, **III-$H_2O$**),[32] with a low conversion to azobenzene (~20%). The slower reduction of **II** by DPH relative to **IV** is consistent with distinct reductive stability profiles of these $Fe(III)_2(\mu\text{-}O)_2$ cores as a result of secondary sphere H-bonding interactions.

The H-bond dependent differences in reaction times for reduction of **II** and **IV** noted above are opposite from

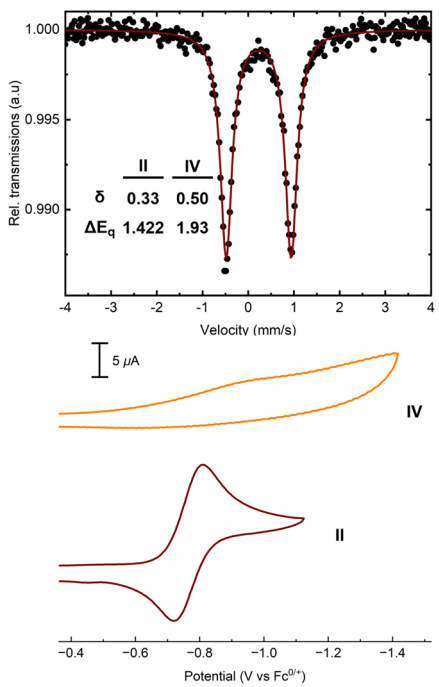

Fig. 3 Top: 298 K Mössbauer spectrum of **II** and associated spectral data for both **II** and **IV**.[26,27] Bottom: cyclic voltammograms of **II** and **IV** (6 mM $[Fe_2(\mu\text{-}O)_2]$, 0.1 M $[Bu_4N][NTf_2]$ in MeCN, 100 mV s^{-1}).

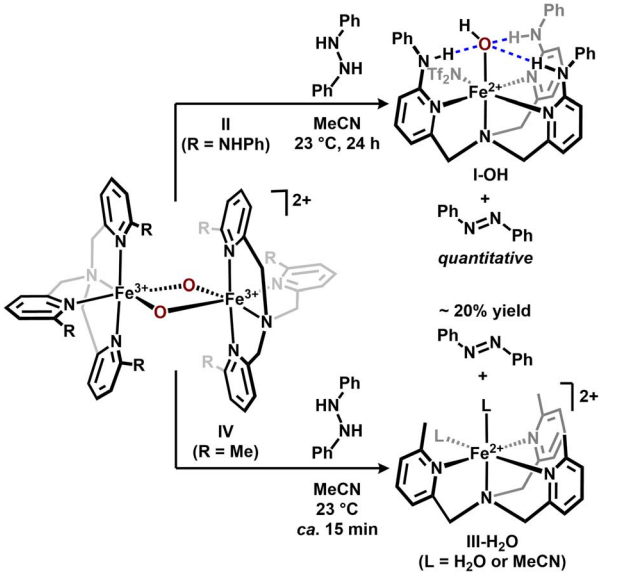

Fig. 4 Reductions of **II** and **IV** with 1,2-diphenylhydrazine (DPH).

observations in Fig. 2 (NO_2^- reactivity). To investigate the role of H-bonds during the initial NO_2^- reduction step, we examined reactions between NO_2^- and the control compound $TPA^{Me}Fe(NTf_2)_2$ (**III-NTf$_2$**), which maintains a similar primary sphere environment to **I-NTf$_2$** but does not contain secondary sphere H-bonds (Fig. 1b).[13b] Introduction of excess (*ca.* 10 equiv.) $[Bu_4N][NO_2]$ to a colorless solution of **III-NTf$_2$** in MeCN immediately produced a yellow solution that exhibited five broad ^{1}H-NMR resonances (assigned as NO_2^- binding). After 7 days, the solution turned orange and developed a characteristic UV-vis shoulder feature at 470 nm, corresponding to **IV** in 93% yield (see SI), and a separate NO trapping experiment provided CoTPP(NO) in 80% yield.

Formation of NO from NO_2^- can occur through multiple distinct pathways (inner- or outer-sphere $2H^+/1e^-$ reduction or through H^+-mediated disproportionation);[33] thus, we executed additional control experiments to provide further clarity into the mechanism for NO_2^- reduction in this system. To probe a disproportionation process, we introduced an exogenous acid, 1-methyl-2-(phenylamino)pyridinium[34] ([HA], Fig. 5), which has a similar structure and charge, and therefore acidity/H-bond donor strength as the appended NHPh groups in **I-NTf$_2$**, to excess $[Bu_4N][NO_2]$ in MeCN. NO did not form in appreciable amounts after 5 h (3% yield of NO (*via* CoTPP(NO)). To examine outer-sphere reduction, we introduced ferrocene[35] to a mixture of 10 equiv. $[Bu_4N][NO_2]$, TPA^{NHPh}, and $Zn(OTf)_2$, and again did not observe NO formation after 5 h. Collectively, these control experiments suggest that neither disproportionation nor outer-sphere reduction pathways proceed at rates comparable to those occurring during NO_2^- reduction with **I-NTf$_2$** or **III-NTf$_2$**. Because the O-atoms from NO_2^- reduction are incorporated into the terminal Fe-containing products (**II** and **IV**), we propose that an inner-sphere reduction pathway is most likely.

Since both **I-NTf$_2$** and **III-NTf$_2$** enabled spontaneous reduction of NO_2^- to NO, we quantified the effects of H-bonds on their kinetic profiles (Fig. 6). Evolution of NO (monitored *via* CoTPP trapping) from a reaction between **I-NTf$_2$** and 10 equiv. $[Bu_4N][NO_2]$ fit well to a first-order exponential model with $k_{obs} = (2.3 \pm 0.2) \times 10^{-4}$ s^{-1}. In contrast, with **III-NTf$_2$**, we observed a slow reaction (linear fit) with $k_{obs} \approx (3) \times 10^{-8}$ s^{-1}, four orders of magnitude slower than **I-NTf$_2$**. To clarify the extent to which the N–O bond cleavage step is promoted by weak Brønsted acids (including the appended NHPh H-bond donors), we performed a control experiment with [HA] and **III-NTf$_2$**. Introduction of 3 equiv. [HA] to a mixture of **III-NTf$_2$** and 10 equiv. $[Bu_4N][NO_2]$ marginally enhanced NO_2^- reduction, affording $k_{obs} = (7.0 \pm 0.9) \times 10^{-8}$ s^{-1} and a concomitant increase in NO yield to 21%

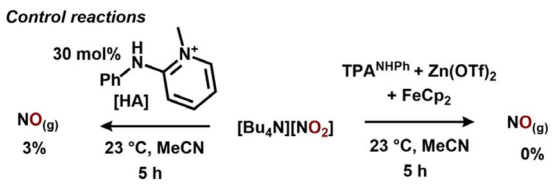

Fig. 5 Assessment of alternative pathways for NO production from NO_2^-.

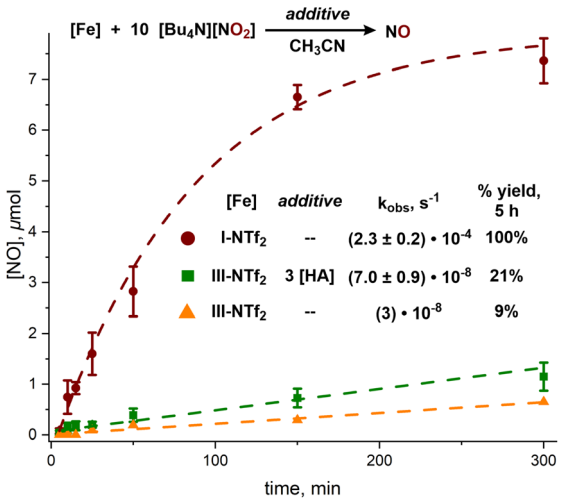

Fig. 6 Kinetic profiles of NO evolution and lines of best fit for NO_2^- reduction with **I-NTf$_2$** (red circles, 1st order exponential fit), **III-NTf$_2$** (orange triangles, linear fit) or **III-NTf$_2$** + 3 equiv. [HA] and 10 equiv. $[NO_2^-]$ (green squares, linear fit). Error bars represent the range of yields from reactions executed in triplicate.

(5 h). These results contrast with the rapid reaction rate and quantitative NO yield (5 h) afforded by **I-NTf$_2$**, suggesting a proximity requirement for the weakly acidic-HNPh groups to provide large rate accelerations for NO_2^- reduction activity as an H-bond donor.

Conclusions

In conclusion, we have reported the first examples of spontaneous NO_2^- reduction to afford $Fe(III)_2(\mu\text{-}O)_2^{2+}$ cores, both in the presence and absence of appended H-bonds (**II** and **IV** respectively). The appended H-bonds within **I-NTf$_2$** provide a four-order of magnitude rate acceleration for NO_2^- reduction, relative to **III-NTf$_2$**, which does not contain H-bonds. Control reactions using exogenous reagents of similar H^+/e^- strengths as **I-NTf$_2$** illustrate the requirement of preorganization of H-bonding units to facilitate rapid nitrite reduction.

The H-bond interactions surrounding the resulting $Fe_2(\mu\text{-}O)_2$ core of **II** imparts distinct electronic and chemical properties relative to **IV**, and as a consequence, **II** is more challenging to reduce with H-atom donors. These observations illustrate the interplay between Fe–O stabilization and subsequent H^+/e^- transfer necessary to promote a net reductive transformation, of particular relevance to nitrite reductases and reaction intermediates containing $Fe_2(\mu\text{-}O)_2$ cores of dioxygenases, as those found in *sMMO*-Q or *RNR*-X. Ongoing work in our lab is focusing on the effects of H-bonds on the electronic structure and reactivity of $Fe(III)_2(\mu\text{-}O)_2$ cores, as well as their application toward catalytic nitrogen-oxyanion reduction.

Author contributions

The manuscript was written through the contributions of all authors. Project conceptualization: J. D. G. and N. K. S.

collection of experimental data: A. R. L., J. E. G., W. S., and J. D. G. Research supervision: N. K. S.

Conflicts of interest

There are no conflicts of interest to declare.

Data availability

CCDC 2448814 and 2448815 contain the supplementary crystallographic data for this paper.[36a,b]

The data supporting this article have been included as part of the SI. Supplementary information: Experimental procedures and characterization of all species and reaction products. See DOI: https://doi.org/10.1039/d5sc04153h.

Acknowledgements

This work was supported by the NIGMS of the NIH under awards R35GM136360 (N. K. S.), and 2R15GM123380-02 (J. D. G). A. R. L. is an NSF-GRFP Fellow (DGE-2241144). Prof. Takele Seda is acknowledged for assistance in obtaining the Mössbauer spectrum of **II**, Dr Reza Loloee at Michigan State University for collection of SQUID magnetometry data, and Prof. Nicolai Lehnert and Claire Patterson for discussions relating to analysis of magnetometry data.

Notes and references

1 L. Ignarro, *Nitric Oxide: Biology and Pathology*, 2000.

2 (*a*) J. Heinecke and P. C. Ford, Mechanistic studies of nitrite reactions with metalloproteins and models relevant to mammalian physiology, *Coord. Chem. Rev.*, 2010, **254**(3), 235–247; (*b*) S. A. Omar and A. J. Webb, Nitrite reduction and cardiovascular protection, *J. Mol. Cell. Cardiol.*, 2014, **73**, 57–69.

3 (*a*) S. L. Rose; S. V. Antonyuk; D. Sasaki; K. Yamashita; K. Hirata; G. Ueno; H. Ago; R. R. Eady; T. Tosha; M. Yamamoto; *et al.*, An unprecedented insight into the catalytic mechanism of copper nitrite reductase from atomic-resolution and damage-free structures. *Sci. Adv.*, 2021, **7**(1), eabd8523; (*b*) S. Rinaldo, G. Giardina, N. Castiglione, V. Stelitano and F. Cutruzzolà, The catalytic mechanism of Pseudomonas aeruginosa cd1 nitrite reductase, *Biochem. Soc. Trans.*, 2011, **39**(1), 195–200; (*c*) S. Besson, M. G. Almeida and C. M. Silveira, Nitrite reduction in bacteria: a comprehensive view of nitrite reductases, *Coord. Chem. Rev.*, 2022, **464**, 214560.

4 (*a*) F. Cutruzzolà, K. Brown, E. K. Wilson, A. Bellelli, M. Arese, M. Tegoni, C. Cambillau and M. Brunori, The nitrite reductase from *Pseudomonas aeruginosa*: essential role of two active-site histidines in the catalytic and structural properties, *Proc. Natl. Acad. Sci. U. S. A.*, 2001, **98**(5), 2232–2237; (*b*) R. Silaghi-Dumitrescu, Linkage Isomerism in Nitrite Reduction by Cytochrome cd1 Nitrite Reductase, *Inorg. Chem.*, 2004, **43**(12), 3715–3718; (*c*) K. Kobayashi, S. Tagawa, Deligeer and S. Suzuki, The pH-Dependent Changes of Intramolecular Electron Transfer on Copper-Containing Nitrite Reductase1, *J. Biochem.*, 1999, **126**(2), 408–412; (*d*) K. Kataoka, H. Furusawa, K. Takagi, K. Yamaguchi and S. Suzuki, Functional Analysis of Conserved Aspartate and Histidine Residues Located Around the Type 2 Copper Site of Copper-Containing Nitrite Reductase1, *J. Biochem.*, 2000, **127**(2), 345–350; (*e*) M. J. Boulanger; M. Kukimoto; M. Nishiyama; S. Horinouchi; M. E. P. Murphy Catalytic Roles for Two Water Bridged Residues (Asp-98 and His-255) in the Active Site of Copper-containing Nitrite Reductase *J. Biol. Chem.* 2000, **275** (31), 23957–23964. DOI: 10.1074/jbc.M001859200, acccessed 2025/05/04; (*f*) N. Xu, J. Yi and G. B. Richter-Addo, Linkage Isomerization in Heme–NO_x Compounds: Understanding NO, Nitrite, and Hyponitrite Interactions with Iron Porphyrins, *Inorg. Chem.*, 2010, **49**(14), 6253–6266.

5 (*a*) Z. Gordon, M. J. Drummond, J. A. Bogart, E. J. Schelter, R. L. Lord and A. R. Fout, Tuning the Fe(II/III) Redox Potential in Nonheme Fe(II)–Hydroxo Complexes through Primary and Secondary Coordination Sphere Modifications, *Inorg. Chem.*, 2017, **56**(9), 4852–4863; (*b*) C. W. J. Lockwood, B. Burlat, M. R. Cheesman, M. Kern, J. Simon, T. A. Clarke, D. J. Richardson and J. N. Butt, Resolution of Key Roles for the Distal Pocket Histidine in Cytochrome c Nitrite Reductases, *J. Am. Chem. Soc.*, 2015, **137**(8), 3059–3068; (*c*) E. T. Judd, N. Stein, A. A. Pacheco and S. J. Elliott, Hydrogen Bonding Networks Tune Proton-Coupled Redox Steps during the Enzymatic Six-Electron Conversion of Nitrite to Ammonia, *Biochemistry*, 2014, **53**(35), 5638–5646.

6 A. S. Borovik, Bioinspired Hydrogen Bond Motifs in Ligand Design: The Role of Noncovalent Interactions in Metal Ion Mediated Activation of Dioxygen, *Acc. Chem. Res.*, 2005, **38**(1), 54–61.

7 (*a*) S. Atta, A. Mandal, R. Saha and A. Majumdar, Reduction of nitrite to nitric oxide and generation of reactive chalcogen species by mononuclear Fe(II) and Zn(II) complexes of thiolate and selenolate, *Dalton Trans.*, 2024, **53**(3), 949–965, DOI: 10.1039/D3DT03768A; (*b*) S. Karmakar, S. Patra, R. Halder, S. Karmakar and A. Majumdar, Reduction of Nitrite in an Iron(II)-Nitrito Compound by Thiols and Selenol Produces Dinitrosyl Iron Complexes *via* an $\{FeNO\}^7$ Intermediate, *Inorg. Chem.*, 2024, **63**(49), 23202–23220; (*c*) Kulbir, S. Das, T. Devi, S. Ghosh, S. Chandra Sahoo and P. Kumar, Acid-induced nitrite reduction of nonheme iron(ii)-nitrite: mimicking biological Fe–NiR reactions, *Chem. Sci.*, 2023, **14**(11), 2935–2942, DOI: 10.1039/D2SC06704H; (*d*) C.-C. Tsou, W.-L. Yang and W.-F. Liaw, Nitrite Activation to Nitric Oxide *via* One-fold Protonation of Iron(II)-*O*,*O*-nitrito Complex: Relevance to the Nitrite Reductase Activity of Deoxyhemoglobin and Deoxyhemerythrin, *J. Am. Chem. Soc.*, 2013, **135**(50), 18758–18761; (*e*) G. Cioncoloni, I. Roger, P. S. Wheatley, C. Wilson, R. E. Morris, S. Sproules and M. D. Symes, Proton-Coupled Electron Transfer Enhances the Electrocatalytic Reduction of Nitrite to NO in a Bioinspired

Copper Complex, *ACS Catal.*, 2018, **8**(6), 5070–5084; (*f*) J. R. Stroka, B. Kandemir, E. M. Matson and K. L. Bren, Electrocatalytic Multielectron Nitrite Reduction in Water by an Iron Complex, *ACS Catal.*, 2020, **10**(23), 13968–13972; (*g*) B. Tran and J. Smith, Nitrogen oxyanion deoxygenation: redox chemistry and oxygen atom transfer reactions, *Coord. Chem. Rev.*, 2025, **530**, 216490.

8 (*a*) A. Sarkar, S. Bhakta, S. Chattopadhyay and A. Dey, Role of distal arginine residue in the mechanism of heme nitrite reductases, *Chem. Sci.*, 2023, **14**(29), 7875–7886, DOI: 10.1039/D3SC01777J; (*b*) J. M. Moore, T. J. Miller, M. Mu, M. N. Peñas-Defrutos, K. L. Gullett, L. S. Elford, S. Quintero, M. García-Melchor and A. R. Fout, Selective Stepwise Reduction of Nitrate and Nitrite to Dinitrogen or Ammonia, *J. Am. Chem. Soc.*, 2025, **147**(10), 8444–8454; (*c*) Y. J. Park, M. N. Peñas-Defrutos, M. J. Drummond, Z. Gordon, O. R. Kelly, I. J. Garvey, K. L. Gullett, M. García-Melchor and A. R. Fout, Secondary Coordination Sphere Influences the Formation of Fe(III)–O or Fe(III)–OH in Nitrite Reduction: A Synthetic and Computational Study, *Inorg. Chem.*, 2022, **61**(21), 8182–8192; (*d*) E. M. Matson, Y. J. Park and A. R. Fout, Facile Nitrite Reduction in a Non-heme Iron System: Formation of an Iron(III)-Oxo, *J. Am. Chem. Soc.*, 2014, **136**(50), 17398–17401; (*e*) K. T. Burns, W. R. Marks, P. M. Cheung, T. Seda, L. N. Zakharov and J. D. Gilbertson, Uncoupled Redox-Inactive Lewis Acids in the Secondary Coordination Sphere Entice Ligand-Based Nitrite Reduction, *Inorg. Chem.*, 2018, **57**(16), 9601–9610; (*f*) A. Mondal, K. P. Reddy, S. Som, D. Chopra and S. Kundu, Nitrate and Nitrite Reductions at Copper(II) Sites: Role of Noncovalent Interactions from Second-Coordination-Sphere, *Inorg. Chem.*, 2022, **61**(50), 20337–20345; (*g*) J. M. Moore and A. R. Fout, Synthetic strategies for oxyanion reduction: metal-based insights and innovations, *Coord. Chem. Rev.*, 2025, **541**, 216692.

9 C. L. Ford, Y. J. Park, E. M. Matson, Z. Gordon and A. R. Fout, A bioinspired iron catalyst for nitrate and perchlorate reduction, *Science*, 2016, **354**(6313), 741–743.

10 (*a*) Y. M. Kwon, M. Delgado, L. N. Zakharov, T. Seda and J. D. Gilbertson, Nitrite reduction by a pyridinediimine complex with a proton-responsive secondary coordination sphere, *Chem. Commun.*, 2016, **52**(73), 11016–11019, DOI: 10.1039/C6CC05962G; (*b*) P. M. Cheung, K. T. Burns, Y. M. Kwon, M. Y. Deshaye, K. J. Aguayo, V. F. Oswald, T. Seda, L. N. Zakharov, T. Kowalczyk and J. D. Gilbertson, Hemilabile Proton Relays and Redox Activity Lead to $\{FeNO\}^{x}$ and Significant Rate Enhancements in NO_2^- Reduction, *J. Am. Chem. Soc.*, 2018, **140**(49), 17040–17050.

11 (*a*) W.-M. Ching, C.-H. Chuang, C.-W. Wu, C.-H. Peng and C.-H. Hung, Facile Nitrite Reduction and Conversion Cycle of $\{Fe(NO)\}^{6/7}$ Species: Chemistry of Iron N-Confused Porphyrin Complexes *via* Protonation/Deprotonation, *J. Am. Chem. Soc.*, 2009, **131**(23), 7952–7953; (*b*) W.-M. Ching, P. P.-Y. Chen and C.-H. Hung, A mechanistic study of nitrite reduction on iron(II) complexes of methylated N-confused porphyrins, *Dalton Trans.*, 2017, **46**(43), 15087–15094, DOI: 10.1039/C7DT02869E.

12 (*a*) Y. Zang, J. Kim, Y. Dong, E. C. Wilkinson, E. H. Appelman and L. Que, Models for Nonheme Iron Intermediates: Structural Basis for Tuning the Spin States of Fe(TPA) Complexes, *J. Am. Chem. Soc.*, 1997, **119**(18), 4197–4205; (*b*) K. A. Jesse and J. S. Anderson, Leveraging ligand-based proton and electron transfer for aerobic reactivity and catalysis, *Chem. Sci.*, 2024, **15**(40), 16409–16423, DOI: 10.1039/D4SC03896G; (*c*) M. R. Elsby, A. Kumar, L. M. Daniels, M. Z. Ertem, N. Hazari, B. Q. Mercado and A. H. Paulus, Linear Free Energy Relationships Associated with Hydride Transfer From $[(6,6'\text{-}R_2\text{-bpy})Re(CO)_3H]$: A Cautionary Tale in Identifying Hydrogen Bonding Effects in the Secondary Coordination Sphere, *Inorg. Chem.*, 2024, **63**(41), 19396–19407; (*d*) J. C. M. Rivas, S. L. Hinchley, L. Metteau and S. Parsons, The strength of hydrogen bonding to metal-bound ligands can contribute to changes in the redox behaviour of metal centres, *Dalton Trans.*, 2006, (19), 2316–2322, DOI: 10.1039/B516234C.

13 (*a*) W. Sarkar, A. LaDuca, J. R. Wilson and N. K. Szymczak, Iron-Catalyzed C–H Oxygenation Using Perchlorate Enabled by Secondary Sphere Hydrogen Bonds, *J. Am. Chem. Soc.*, 2024, **146**(15), 10508–10516; (*b*) A. R. LaDuca, J. R. Wilson, W. Sarkar, M. Zeller and N. K. Szymczak, Impact of Secondary Sphere Hydrogen Bonds on O_2 Reactivity within a Nonheme Iron Complex, *J. Am. Chem. Soc.*, 2025, **147**(6), 5099–5105; (*c*) W. Sarkar and N. K. Szymczak, Expanding Perchlorate Use for C–H Oxidative Transformations: A Tandem Photo- and Iron-Catalytic Strategy, *Organometallics*, 2025, **44**(7), 777–782; (*d*) J. R. Wilson, M. Zeller and N. K. Szymczak, Hydrogen-bonded nickel(I) complexes, *Chem. Commun.*, 2021, **57**(6), 753–756; (*e*) J. P. Shanahan, D. M. Mullis, M. Zeller and N. K. Szymczak, Reductively Stable Hydrogen-Bonding Ligands Featuring Appended CF_2–H Units, *J. Am. Chem. Soc.*, 2020, **142**(19), 8809–8817, DOI: 10.1021/jacs.0c01718; (*f*) E. W. Dahl, J. J. Kiernicki, M. Zeller and N. K. Szymczak, Hydrogen Bonds Dictate O_2 Capture and Release within a Zinc Tripod, *J. Am. Chem. Soc.*, 2018, **140**(32), 10075–10079; (*g*) E. W. Dahl, H. T. Dong and N. K. Szymczak, Phenylamino derivatives of tris(2-pyridylmethyl)amine: hydrogen-bonded peroxodicopper complexes, *Chem. Commun.*, 2018, **54**(8), 892–895, DOI: 10.1039/C7CC08619A; (*h*) E. W. Dahl and N. K. Szymczak, Hydrogen Bonds Dictate the Coordination Geometry of Copper: Characterization of a Square-Planar Copper(I) Complex, *Angew. Chem., Int. Ed.*, 2016, **55**(9), 3101–3105.

14 C. M. Moore and N. K. Szymczak, Nitrite reduction by copper through ligand-mediated proton and electron transfer, *Chem. Sci.*, 2015, **6**(6), 3373–3377, DOI: 10.1039/C5SC00720H.

15 A. V. Iogansen, Direct proportionality of the hydrogen bonding energy and the intensification of the stretching ν(XH) vibration in infrared spectra, *Spectrochim. Acta, Part A*, 1999, **55**(7), 1585–1612.

16 Relative to **I-NTf$_2$**, the reaction evolved 1 equivalent of NO gas.

17 We propose that the dimeric structure of **II** stays intact in solution because variable temperature ^{1}H-NMR spectroscopy of **II** in MeCN did not display significant changes between +80 to −35 °C.

18 (*a*) A. J. Jasniewski and L. Que Jr, Dioxygen Activation by Nonheme Diiron Enzymes: Diverse Dioxygen Adducts, High-Valent Intermediates, and Related Model Complexes, *Chem. Rev.*, 2018, **118**(5), 2554–2592; (*b*) R. Banerjee, J. C. Jones and J. D. Lipscomb, Soluble Methane Monooxygenase, *Annu. Rev. Biochem.*, 2019, **88**, 409–431; (*c*) A. B. Jacobs, R. Banerjee, D. E. Deweese, A. Braun, J. T. Babicz Jr, L. B. Gee, K. D. Sutherlin, L. H. Böttger, Y. Yoda, M. Saito, *et al.*, Nuclear Resonance Vibrational Spectroscopic Definition of the Fe(IV)$_2$ Intermediate Q in Methane Monooxygenase and Its Reactivity, *J. Am. Chem. Soc.*, 2021, **143**(39), 16007–16029; (*d*) B. E. Sturgeon, D. Burdi, S. Chen, B.-H. Huynh, D. E. Edmondson, J. Stubbe and B. M. Hoffman, Reconsideration of X, the Diiron Intermediate Formed during Cofactor Assembly in *E. coli* Ribonucleotide Reductase, *J. Am. Chem. Soc.*, 1996, **118**(32), 7551–7557.

19 (*a*) D. Kass, S. Yao, K. B. Krause, T. Corona, L. Richter, T. Braun, S. Mebs, M. Haumann, H. Dau, T. Lohmiller, *et al.*, Spectroscopic Properties of a Biologically Relevant [Fe$_2$(μ-O)$_2$] Diamond Core Motif with a Short Iron-Iron Distance, *Angew. Chem., Int. Ed.*, 2023, **62**(10), e202209437; (*b*) H. Zheng, Y. Zang, Y. Dong, V. G. Young and L. Que, Complexes with FeIII$_2$(μ-O)(μ-OH), FeIII$_2$(μ-O)$_2$, and [FeIII$_3$(μ$_2$-O)$_3$] Cores: Structures, Spectroscopy, and Core Interconversions, *J. Am. Chem. Soc.*, 1999, **121**(10), 2226–2235; (*c*) Y. Honda, H. Arii, T. Okumura, A. Wada, Y. Funahashi, T. Ozawa, K. Jitsukawa and H. Masuda, Complexes with FeIII$_2$(μ-O)(μ-OH) Core Surrounded by Hydrogen-Bonding Interaction, *Bull. Chem. Soc. Jpn.*, 2007, **80**(7), 1288–1295; (*d*) G. T. Rohde, G. Xue and L. Que, Explorations of the nonheme high-valent iron-oxo landscape: crystal structure of a synthetic complex with an [FeIV$_2$(μ-O)$_2$] diamond core relevant to the chemistry of sMMOH, *Faraday Discuss.*, 2022, **234**, 109–128, DOI: 10.1039/D1FD00066G; (*e*) H.-F. Hsu, Y. Dong, L. Shu, V. G. Young and L. Que, Crystal Structure of a Synthetic High-Valent Complex with an Fe$_2$(μ-O)$_2$ Diamond Core. Implications for the Core Structures of Methane Monooxygenase Intermediate Q and Ribonucleotide Reductase Intermediate X, *J. Am. Chem. Soc.*, 1999, **121**(22), 5230–5237; (*f*) L. Fohlmeister, K. R. Vignesh, F. Winter, B. Moubaraki, G. Rajaraman, R. Pöttgen, K. S. Murray and C. Jones, Neutral diiron(iii) complexes with Fe$_2$(μ-E)$_2$ (E = O, S, Se) core structures: reactivity of an iron(I) dimer towards chalcogens, *Dalton Trans.*, 2015, **44**(4), 1700–1708, DOI: 10.1039/C4DT03081H; (*g*) Y. Zang, Y. Dong, L. Que Jr, K. Kauffmann and E. Muenck, The First Bis(.mu.-oxo) diiron(III) Complex. Structure and Magnetic Properties of [Fe$_2$(.mu.-O)$_2$(6TLA)$_2$](ClO$_4$)$_2$, *J. Am. Chem. Soc.*, 1995, **117**(3), 1169–1170; (*h*) Y. Mikata, Y. Aono, C. Yamamoto, H. Nakayama, A. Matsumoto, F. Kotegawa, M. Harada, H. Katano, Y. Kobayashi, S. Yanagisawa, *et al.*, A Synthetic Model for the Possible FeIV$_2$(μ-O)$_2$ Core of Methane Monooxygenase Intermediate Q Derived from a Structurally Characterized FeIIIFeIV(μ-O)$_2$ Complex, *Inorg. Chem.*, 2022, **61**(2), 786–790; (*i*) P. Zhao, H. Lei, C. Ni, J.-D. Guo, S. Kamali, J. C. Fettinger, F. Grandjean, G. J. Long, S. Nagase and P. P. Power, Quasi-Three-Coordinate Iron and Cobalt Terphenoxide Complexes {Ar^{iPr8}OM(μ-O)}$_2$ (Ar^{iPr8} = C$_6$H-2,6-(C$_6$H$_2$-2,4,6-iPr$_3$)$_2$-3,5-iPr$_2$; M = Fe or Co) with M(III)$_2$(μ-O)$_2$ Core Structures and the Peroxide Dimer of 2-Oxepinoxy Relevant to Benzene Oxidation, *Inorg. Chem.*, 2015, **54**(18), 8914–8922.

20 The structure of **IV** reported in this work is used for comparing structural metrics because it is of higher quality than the previous polymorph (R_1 = 3.95% *versus* R_1 = 6.5% in ref. 19g).

21 A. Dey, R. K. Hocking, P. Larsen, A. S. Borovik, K. O. Hodgson, B. Hedman and E. I. Solomon, X-ray Absorption Spectroscopy and Density Functional Theory Studies of [(H$_3$buea)FeIII–X]$^{n-}$ (X = S^{2-}, O^{2-}, OH^{-}): Comparison of Bonding and Hydrogen Bonding in Oxo and Sulfido Complexes, *J. Am. Chem. Soc.*, 2006, **128**(30), 9825–9833.

22 V. F. Oswald, J. L. Lee, S. Biswas, A. C. Weitz, K. Mittra, R. Fan, J. Li, J. Zhao, M. Y. Hu, E. E. Alp, *et al.*, Effects of Noncovalent Interactions on High-Spin Fe(IV)–Oxido Complexes, *J. Am. Chem. Soc.*, 2020, **142**(27), 11804–11817.

23 (*a*) G. J. Long and F. Grandjean, 2.20 – Mössbauer Spectroscopy: Introduction, in *Comprehensive Coordination Chemistry II*, ed. McCleverty, J. A. and Meyer, T. J., Pergamon, 2003, pp. 269–277; (*b*) We tabulated the bond metrics and Mössbauer parameters of biological and synthetic Fe$_2$(μ-O)$_2$ cores (see Table S1). The spectral parameters for **II** are similar to the complexes in ref. 19a, f, and i.

24 E. Zars, L. Gravogl, M. R. Gau, P. J. Carroll, K. Meyer and D. J. Mindiola, Isostructural bridging diferrous chalcogenide cores [FeII(μ-E)FeII] (E = O, S, Se, Te) with decreasing antiferromagnetic coupling down the chalcogenide series, *Chem. Sci.*, 2023, **14**(24), 6770–6779, DOI: 10.1039/D3SC01094E.

25 (*a*) The temperature-dependent magnetic susceptibility of **II** (SQUID) was modelled with the exchange Hamiltonian $\hat{H}_{ex} = -J \times S_1S_2$ using Easyspin's curry function.; (*b*) S. Stoll and A. Schweiger, EasySpin, a comprehensive software package for spectral simulation and analysis in EPR, *J. Magn. Reson.*, 2006, **178**(1), 42–55.

26 The Mössbauer spectrum of **II** (as a polycrystalline solid) was collected at 298 K using a constant-acceleration spectrometer (Wissel GMBH, Germany) in a horizontal transmission mode using a 50 mCi $_{57}$Co source was utilized for Mössbauer spectra collection. All Mössbauer spectra were collected at room temperature at 4 mm s^{-1} velocity with approximately 80 mg of sample loaded into an acrylic sample holder with minimal Paratone-N oil to prevent oxidation. Lorentzian line shape with the NORMOS (Wissel GMBH) least-squares fitting program was used to fit spectra, and isomer shifts were normalized to

metallic iron. We attribute the slight asymmetry in the two peaks to the random orientation of the polycrystalline sample. See ref. 27.

27 E. Kreber and U. Gonser, The Problem of Texture in Mössbauer Spectroscopy, *Texture, Stress, Microstruct.*, 1974, **1**(4), 869318.

28 At −40 °C, the CV of **IV** has been reported to feature a reversible Fe(III)$_2$ to Fe(III)Fe(IV) wave ($E^{1/2} = 0.41$ V) that we did not observe at ambient temperature. See ref. 29.

29 H. Zheng, S. J. Yoo, E. Münck and L. Que, The Flexible Fe$_2$(μ-O)$_2$ Diamond Core: A Terminal Iron(IV)−Oxo Species Generated from the Oxidation of a Bis(μ-oxo)diiron(III) Complex, *J. Am. Chem. Soc.*, 2000, **122**(15), 3789–3790.

30 J. J. Warren, T. A. Tronic and J. M. Mayer, Thermochemistry of Proton-Coupled Electron Transfer Reagents and its Implications, *Chem. Rev.*, 2010, **110**(12), 6961–7001.

31 Treatment of **II** with substrates containing weak C–H bonds (*i.e.* 9,10-dihydroanthracene or Ph_3CH) as reductants did not afford reduction of **II** nor C–H oxidation (to form anthracene, anthraquinone, or Ph_3COH). See SI for further details.

32 S. V. Kryatov, E. V. Rybak-Akimova, V. L. MacMurdo and L. Que, A Mechanistic Study of the Reaction between a Diiron(II) Complex $[FeII_2(\mu\text{-}OH)_2(6\text{-}Me_3\text{-}TPA)_2]^{2+}$ and O_2 to Form a Diiron(III) Peroxo Complex, *Inorg. Chem.*, 2001, **40**(10), 2220–2228.

33 (*a*) M. Knipp and C. He, Nitrophorins: nitrite disproportionation reaction and other novel functionalities of insect heme-based nitric oxide transport proteins, *IUBMB Life*, 2011, **63**(5), 304–312; (*b*) M. S. Rayson, J. C. Mackie, E. M. Kennedy and B. Z. Dlugogorski, Accurate Rate Constants for Decomposition of Aqueous Nitrous Acid, *Inorg. Chem.*, 2012, **51**(4), 2178–2185; (*c*) V. Hosseininasab, I. M. DiMucci, P. Ghosh, J. A. Bertke, S. Chandrasekharan, C. J. Titus, D. Nordlund, J. H. Freed, K. M. Lancaster and T. H. Warren, Lewis acid-assisted reduction of nitrite to nitric and nitrous oxides *via* the elusive nitrite radical dianion, *Nat. Chem.*, 2022, **14**(11), 1265–1269.

34 1-Methyl-2-(phenylamino)pyridinium [HA] features an ν(NH) band at 3272 cm^{-1}, while **I-NTf$_2$**'s ν(NH) is at 3278 cm^{-1} (see SI). This further supports our assertion that [HA] and **I-NTf$_2$** have similar acidity/H-bond donor strengths.

35 We selected ferrocene as a reductant in this control reaction because it approximates the reducing potential of **I-NTf$_2$** and **III-NTf$_2$** in the presence of 10 equiv. $[Bu_4N][NO_2]$ (0.05 V *vs.* $Fc^{0/+}$) see SI.

36 (*a*) A. R. LaDuca, J. E. Gonder, W. Sarkar, J. D. Gilbertson and N. Szymczak, CCDC 2448814: Experimental Crystal Structure Determination, 2025, DOI: 10.5517/ccdc.csd.cc2n6603; (*b*) A. R. LaDuca, J. E. Gonder, W. Sarkar, J. D. Gilbertson and N. Szymczak, CCDC 2448815: Experimental Crystal Structure Determination, 2025, DOI: 10.5517/ccdc.csd.cc2n6614.